Code-division SQUID multiplexing

M. D. Niemack,[1,a)] J. Beyer,[2] H. M. Cho,[1] W. B. Doriese,[1] G. C. Hilton,[1] K. D. Irwin,[1] C. D. Reintsema,[1] D. R. Schmidt,[1] J. N. Ullom,[1] and L. R. Vale[1]
[1]*National Institute of Standards and Technology, 325 Broadway, MC 817.03, Boulder, Colorado 80305, USA*
[2]*Physikalisch-Technische Bundesanstalt (PTB), Abbestraße 2-12, D-10587 Berlin, Germany*

(Received 13 December 2009; accepted 12 March 2010; published online 23 April 2010)

Multiplexed superconducting quantum interference device (SQUID) readout systems are critical for measuring large arrays of superconducting transition-edge sensors (TES). We demonstrate a code-division SQUID multiplexing (CDM) architecture that is modulated by Walsh codes. Measurements and simulations of a prototype multiplexer show that this modulation scheme is not degraded by SQUID-noise aliasing, suppresses parasitic pickup, and has low levels of crosstalk. These properties enable this architecture to scale to large TES arrays. Furthermore, CDM modulation suppresses the $1/f$ knee in the noise to below 20 mHz, suggesting the use of this circuit for low-frequency-noise mitigation in more general SQUID applications. © *2010 American Institute of Physics*. [doi:10.1063/1.3378772]

Transition-edge sensor (TES) detectors have recently enabled remarkable improvements in radiation measurements spanning eight orders of magnitude in wavelength.[1] TES bolometers are being used in kilopixel-scale arrays for millimeter-wave astrophysics, and TES microcalorimeters hold energy resolution records for nondispersive detectors over a wide range of energy scales. Multiplexed superconducting quantum interference device (SQUID) readout is an integral technology to these developments and will become ever more essential as array sizes continue to increase. Two SQUID multiplexing techniques currently read out large TES arrays: time-division multiplexing[2] (TDM) and frequency-division multiplexing[3] (FDM). These techniques are limited in the number of detectors, N, that can be read out per column by different mechanisms. In TDM, N is limited by SQUID-noise aliasing, which increases as $\sqrt{N}$, and in large N readout of microcalorimeters, energy resolution can be degraded by insufficient knowledge of pulse arrival times. Currently deployed FDM systems operate at megahertz frequencies at which N is constrained by crosstalk in compact, narrow-band filters. A different technique under development to improve FDM readout will operate at gigahertz frequencies.[4] In this letter, we present a code-division multiplexing (CDM) architecture that combines advantages of TDM and FDM, and is expected to enable multiplexing of substantially larger TES arrays. We describe the testing results of a four row prototype code-division multiplexer.

In any multiplexing scheme, a set of modulation functions combines and reseparates the signals. In TDM these functions are N low-duty-cycle square waves; in FDM they are N sinusoids at different frequencies.

In this implementation of CDM, N detector signals have the polarity of their coupling to a SQUID amplifier modulated by Walsh functions,[5] for which N must be a power of two. For the $N=4$ demonstration described in this letter, the Walsh matrix is

$$W \equiv \begin{pmatrix} 1 & 1 & 1 & 1 \\ 1 & 1 & -1 & -1 \\ 1 & -1 & -1 & 1 \\ 1 & -1 & 1 & -1 \end{pmatrix} = 4\ W^{-1}. \tag{1}$$

The matrix columns indicate time steps during an N step data frame; we denote these Walsh states as a, b, c, and d. Each row of the matrix is a Walsh function that is applied to a different row of pixels. The signals from individual rows are decoded from the raw column output by multiplying each frame of data comprising N samples by the inverse the matrix, W^{-1}. Similarly to TDM,[2] CDM is designed such that rows of pixels are modulated via row address lines, and columns are read out in parallel. The demonstration described here involves one column and four rows, so each row consists of a single pixel (Fig. 1).

The first row in the Walsh matrix maintains constant polarity throughout the data frame. This nonswitched row gives an essential measurement of common coherent noise sources, which are suppressed in the switched rows by alternating the signal polarity.

In both TDM and CDM, the open-loop bandwidth must be at least the inverse of the row-switching period in order that switching transients settle before sampling.[6,7] In TDM, the equivalent modulation matrix to W is the identity matrix. Thus, TDM rows are only sampled once per frame and are off for the rest of the frame, leading to an increase in SQUID noise by $\sqrt{N}$ due to aliasing.[2] A primary advantage of CDM is that it does not suffer from this aliasing because all rows are sampled every switching cycle, so the detector signal also increases by $\sqrt{N}$. A second advantage is that subframe sampling can be used to reconstruct pulse arrival times for microcalorimeters on the Walsh-switching time scale (typically less than 1 μs, with a goal of 160 ns) rather than the frame time scale, which will aid in alignment of pulses with the optimal-filter template. An advantage of this implementation of CDM is less stringent SQUID fabrication requirements because the optimal row address currents are determined by geometrical couplings as opposed to critical currents. This

a)Electronic mail: niemack@nist.gov.

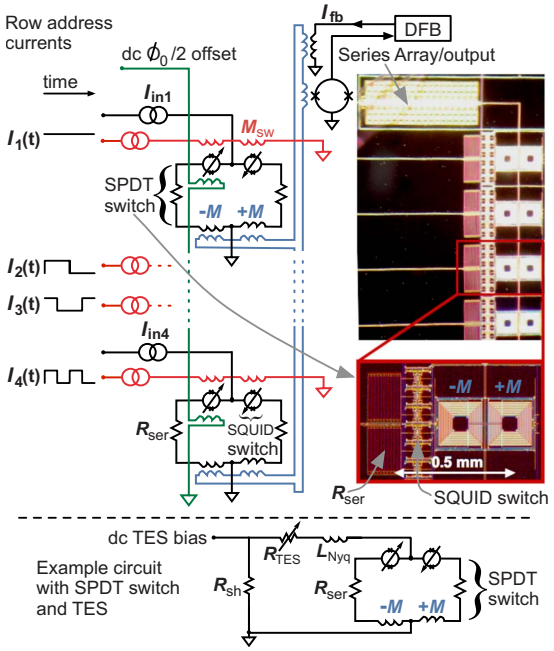

FIG. 1. (Color online) Top: Schematic and photographs of a four-row code-division multiplexer. The dc $\phi_0/2$ flux offset is applied to one of the two SQUID switches in each SPDT switch. The row address lines (I_1, I_2, I_3, I_4) then modulate the flux in each SPDT by switching between zero or $\phi_0/2$ flux. The result is that one half of the SPDT switch is open, while the other half is closed, so the input signal, I_{in}, couples to the summing coil through either $-M$ or $+M$. The row address currents are orthogonal Walsh functions as shown to the left of the schematic. The signals from all SPDT switches are coupled to the SA SQUID amplifier through a summing coil. Room temperature digital-feedback electronics (DFB) are used to servo the feedback current, I_{fb}, which keeps the SA output in its linear regime. The second dimension of CDM would come from common row addressing lines for multiple CDM columns (not shown, but similar to TDM). Bottom: Schematic of SPDT integrated with a TES, showing how a dc biased TES can be connected to an SPDT switch with the same components used in TDM systems: a Nyquist inductor, L_{Nyq}, to limit the TES bandwidth and a shunt resistor, $R_{sh} \ll R_{TES}$, to provide a hard voltage bias for the TES.

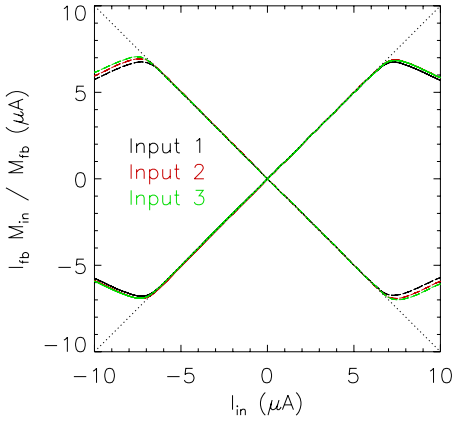

FIG. 2. (Color online) SPDT switch *I-I* curve measurements: normalized feedback current, $I_{fb}M_{in}/M_{fb}$, vs input current, I_{in}. Positive (solid) and negative (dashed) polarity switch *I-I* curves are shown for three inputs. The linear region between ± 6 μA is where one SQUID switch remains superconducting, while the inflection points near ± 7 μA are indicative of the SQUID switch critical currents and the transition to the normal state. These data are used to extract the switch-to-SA mutual inductance ($M_{in} = 35.6 \pm 0.2$ pH), the switch mutual inductance ($M_{sw} = 1.95 \pm 0.03$ pH), and the consistency of the SPDT coupling for all rows ($M_{fb}/M_{in} = 0.731 \pm 0.003$ for both slopes of three input channels). The independent integral linearity error of all SQUID switch *I-I* curves was measured to be smaller than 1% between ± 6 μA.

architecture requires only minor firmware modifications to existing room-temperature TDM electronics.

Previous attempts to implement CDM with TESs have switched the polarity of the TES bias line,[8,9] which results in aliasing of detector noise by the factor $\sqrt{N}$, due to the large bandwidth in the TES loop required to enable fast polarity switching. This implementation prevents detector-noise aliasing by separating the high-bandwidth switching circuit from the low-pass filtered detector bias circuit. The TES bandwidth is limited to a few kilohertz by use of an L/R filter (Fig. 1). The polarity switching is accomplished by use of a single-pole double-throw (SPDT) current-steering switch that comprises two parallel circuits, each containing a low-inductance SQUID, a series resistor, R_{ser}, and a transformer that couples the signal to the summing coil (Fig. 1). The low-inductance SQUIDs (henceforth SQUID switches) have a critical current that approaches zero for $\phi_0(n+1/2)$ values of magnetic flux, where n is an integer.[10] Application of a dc $\phi_0/2$ flux offset to one of the SQUID switches in each SPDT minimizes the critical current of that SQUID switch, and the TES (or other input) current drives it normal ($R_N \approx 2$ Ω). The other SQUID switch, with a higher critical current, superconducts and the current through $R_{ser} \approx 9$ mΩ generates a voltage bias across the normal SQUID switch. Because $R_N \gg R_{ser}$, the normal SQUID switch is "open," while the superconducting SQUID switch is "closed." The coupling of the detector signal to the summing coil is reversed from $+M$ to $-M$ by applying an additional $\phi_0/2$ to both SQUID switches via the row-address lines, which interchanges the normal and superconducting states. The readout SQUID is an amplifying series array (SA) of SQUIDs that connects to a room-temperature preamplifier and to digital feedback (DFB) electronics.[6]

Prototype four-row CDM multiplexers have been fabricated (Fig. 1) and tested in a liquid He dip probe. SA *V-*ϕ and *I-V* curves are measured to determine the SQUID critical current ($I_{c\text{-}max} = 7.6 \pm 0.2$ μA) and the feedback coil mutual inductance ($M_{fb} = 26.0 \pm 0.1$ pH), and to estimate the power dissipation for a single column (less than 1 nW). Dissipation in the SQUID switches is predicted to be negligible compared to the SA dissipation and similar to the TES bias power. SQUID switch *I-I* curves (Fig. 2) are measured by application of a $\phi_0/2$ offset to one of the SQUID switches followed by applying an additional $\phi_0/2$ row-address to switch the polarity of the SPDT. The linear dynamic range of the input in this implementation of CDM is limited by the maximum SQUID switch critical current (Fig. 2). While the prototype circuit described here was designed primarily to test this CDM implementation and is appropriate for use with relatively low-current (less than 6 μA) signals, the next generation of CDM chip under development will be designed for higher current applications.

When the readout is multiplexed, the amplified SA output is connected to DFB electronics[6] that apply polarity-modulating row-addresses synchronously with interleaved proportional-integral (PI) feedback values for each Walsh state. Measurements of row-switching settling periods indicate that row-switching rates greater than 1 MHz are possible with this circuit. To facilitate low-frequency noise measurements, a passive $f_{3dB} \approx 200$ kHz filter was used to limit the open-loop bandwidth of the SA output. The four-row multiplexing tests described here were carried out with a 200 kHz switching rate, and thus a 50 kHz frame rate.

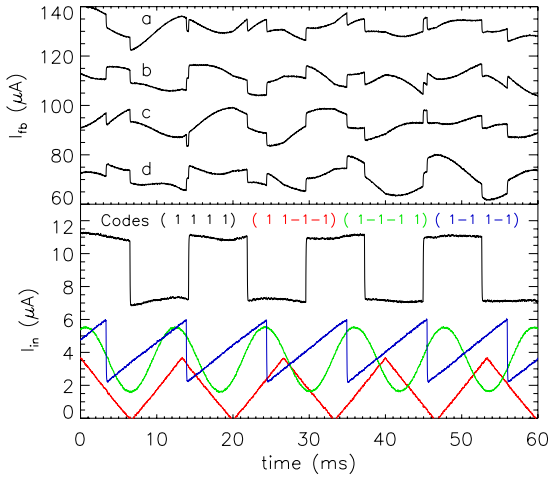

FIG. 3. (Color online) Demonstration of four-row CDM. Top: Raw DFB data, I_{fb}. The four sequential Walsh states (a,b,c,d) are interleaved in time. There is an arbitrary offset in the feedback data; however, the relative dc levels enable extraction of the dc current for all switched rows. (States "c" and "d" have been shifted down by 25 μA and 45 μA, respectively, for clarity.) Bottom: Decoded signals converted into units of I_{in}. The square-wave signal input to the nonswitched pixel (black) clearly shows more drift and pickup than the three switched signals (triangle, sinusoid, and ramp). The dc offsets of the switched signals are properly calibrated after decoding, while the nonswitched signal contains an arbitrary SQUID readout offset.

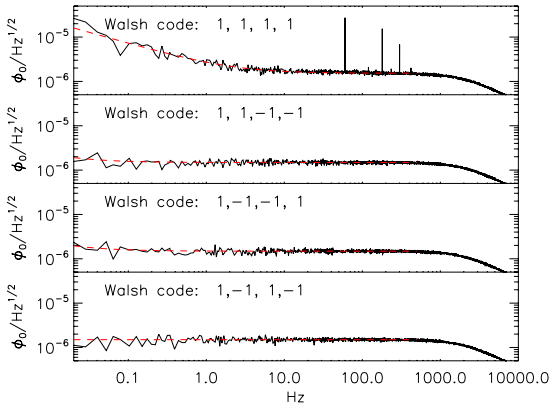

FIG. 4. (Color online) Noise measurements of a four-row CDM multiplexer. Each panel shows Fourier transformed data from one of the decoded Walsh functions, or rows, as specified in the legend. The polarity switching rows have strongly suppressed $1/f$ knees and pickup of parasitic lines compared to the nonswitching (top) row. Fits to the data below 500 Hz (dashed lines) indicate that the nonswitching row has a $1/f$ knee at ~2.2 Hz (consistent with nonmultiplexed noise measurements), while the switching rows show no evidence of a $1/f$ knee above 20 mHz. The data also confirm that there is no SQUID noise aliasing degradation due to the number of multiplexed rows. The low-pass filtering apparent near ~5 kHz is due to the PI term amplitudes in the feedback loop.

To demonstrate the CDM functionality, signal generators were used to apply different signals to all four input lines while multiplexing. Figure 3 shows the raw DFB data for the four Walsh states as well as the decoded data after applying W^{-1} (Eq. (1)) to the raw data. Low-frequency SQUID noise, noise-pickup lines, and the arbitrary dc SQUID offset are all generally confined to the nonswitched row. The multiplexed noise measurements in Fig. 4 were acquired with no signals on the inputs to demonstrate the reduction of all of these effects on the switched rows. The nonswitched row contains a $1/f$ knee at ~2.2 Hz as well as parasitic pickup lines at 60 Hz and harmonics, which are consistent with nonmultiplexed measurements of the SQUID noise. The switched rows show no evidence of parasitic pickup or a $1/f$ knee above 20 mHz. Due to the 200 kHz filter on the output line combined with sparse data sampling after the settling time by the DFB electronics, the measured white noise level of 1.50 ± 0.04 $\mu\phi_0/\mathrm{Hz}^{1/2}$ is degraded by $\pi^{1/2}$ relative to the nonmultiplexed white noise level[7] of 0.9 ± 0.1 $\mu\phi_0/\mathrm{Hz}^{1/2}$; however, there is no SQUID-noise degradation due to increasing the number of rows.

Crosstalk in Walsh space has been simulated and measured by application of sine-wave signals between 1 Hz and 25 kHz to the inputs, and comparing the power spectral densities of the decoded time streams of all rows at the sine-wave frequencies. The measurements and simulations are consistent. After implementing a simple algorithm during decoding to remove linear drift within data frames, we find that crosstalk between all channels is suppressed at 100 (1000) Hz to between −90 (−50) dB and −106 (−66) dB for a frame rate of 50 kHz. Measurements of the nonswitched row have larger crosstalk than predicted from the simulations, which is expected, due to parasitic magnetic crosstalk between pixels that is not suppressed in the nonswitched row. In CDM implementations with detectors, this row will be used for characterization of amplifier noise and parasitic pickup and will not be connected to a detector.

We have demonstrated a functional code-division SQUID multiplexer that is not degraded by $\sqrt{N}$ SQUID noise aliasing. Our measurements show that CDM suppresses parasitic pickup and SQUID $1/f$ in the readout circuit and preclude a $1/f$ knee above 20 mHz on the switching rows. These qualities make the CDM implementation described here attractive for general SQUID applications with strict noise requirements. In addition, because the rows are switched by use of magnetic flux, future versions of this CDM have the potential to take advantage of binary addressing in which 2^n, rows are modulated by n addressing lines.[11] Our next generation of CDM chips will include a larger number of rows and will target higher SQUID-switch critical currents and mutual inductances for use with TES.

This work was supported in part by NASA under Contract No. NNG09WF27I. and a National Research Council Postdoctoral Fellowship (Niemack).

[1] K. D. Irwin and G. C. Hilton, *Cryogenic Particle Detection: Transition-Edge Sensors*, edited by C. Enss (Springer, Berlin, 2005).
[2] J. A. Chervenak, K. D. Irwin, E. N. Grossman, J. M. Martinis, C. D. Reintsema, and M. E. Huber, Appl. Phys. Lett. **74**, 4043 (1999).
[3] J. Yoon, J. Clarke, J. M. Gildemeister, A. T. Lee, M. J. Myers, P. L. Richards, and J. T. Skidmore, Appl. Phys. Lett. **78**, 371 (2001).
[4] J. A. B. Mates, G. C. Hilton, K. D. Irwin, L. R. Vale, and K. W. Lehnert, Appl. Phys. Lett. **92**, 023514 (2008).
[5] J. L. Walsh, Am. J. Math. **45**, 5 (1923).
[6] C. D. Reintsema, J. Beyer, S. W. Nam, S. Deiker, G. C. Hilton, K. Irwin, J. Martinis, J. Ullom, L. R. Vale, and M. MacIntosh, Rev. Sci. Instrum. **74**, 4500 (2003).
[7] W. B. Doriese, J. A. Beall, W. D. Duncan, L. Ferreira, G. C. Hilton, K. D. Irwin, C. D. Reintsema, J. N. Ullom, L. R. Vale, and Y. Xu, Nucl. Instrum. Methods Phys. Res. A **559**, 808 (2006).
[8] B. Karasik and W. McGrath, Proceedings of the 12th International Symposium on Space Terahertz Technology, 2001, pp. 436–445.
[9] M. Podt, J. Weenink, J. Flokstra, and H. Rogalla, Physica C **368**, 218 (2002).
[10] J. Beyer and D. Drung, Supercond. Sci. Technol. **21**, 105022 (2008).
[11] K. D. Irwin, M. D. Niemack, J. Beyer, H. M. Cho, W. B. Doriese, G. C. Hilton, C. D. Reintsema, D. R. Schmidt, J. N. Ullom, and L. R. Vale, Supercond. Sci. Technol. **23**, 034004 (2010).